Accuracy Evaluation of the FY-4A AGRI Land Surface Temperature Product

Yiyao Gao, Shanyou Zhu, Guixin Zhang, and Yongming Xu

***Abstract*—Land surface temperature (LST) plays a key role in surface-atmosphere interactions and energy exchange processes and is an important parameter indispensable for earth science research. The LST accuracy retrieved from the Advanced Geosynchronous Radiation Imager (AGRI) onboard China's geostationary meteorological satellite FY-4A has not been well evaluated, which affects its further applications. In this article, the accuracy of AGRI land surface temperature products is evaluated by a direct verification method using land surface temperature data observed at meteorological stations in China. On this basis, the angle correction kernel model is used to perform angle correction for AGRI LST products by comparing the angle difference between AGRI and moderate-resolution imaging spectroradiometer (MODIS) sensor imaging moments, and MOD11A1 products in central China are selected to cross-validate the accuracy of AGRI LST products. The results show that the spatial and temporal distributions of AGRI land surface temperature and meteorological station observations are consistent, and the accuracy of AGRI LST differs somewhat in different seasons, with the lowest correlation of 0.68 and root-mean-square error (RMSE) of 10.92 K in Summer, and 0.89 and 6.89 K in Winter. The correlation between AGRI LST and MOD11A1 LST before angle correction is 0.64, and the RMSE is 5.45 K. After angle correction, the correlation increases to 0.90, and the RMSE decreases by 2.12 K. There are differences in the angle correction results for various land cover types and different terrains, and the accuracy of AGRI LST at the time of the ascending track (nighttime) is higher than that of the descending track (daytime). The overall results of direct verification and cross-validation indicate that FY-4A AGRI LST product has high accuracy and can accurately express the spatial and temporal distribution characteristics and variation patterns of land surface temperature.**

***Index Terms*—Angle correction, cross-validation, direct verification, land surface temperature (LST), moderate-resolution imaging spectroradiometer (MODIS).**

I. Introduction

LAND surface temperature (LST) is an important parameter for the radiative balance of the coupled surface-atmosphere system and physical processes at the surface [1]. The Global Climate Observing System organization and the Climate Change Initiative of the European Space Agency specify land surface temperature as one of the essential climate variables for monitoring the earth's climate system. Essential climate variables [2] and their spatio-temporal variability information are of great scientific significance and application value in the fields of weather prediction, climate change, water cycle, geological exploration, agriculture and forestry monitoring, and urban thermal environment [3], [4], [5]. Remote sensing, especially thermal infrared remote sensing, as the main technology to obtain LST at regional and global scales, has received extensive attention in recent years. The further application of LST products mainly depend on their data quality, and understanding the accuracy of remote sensing retrieved LST products is an important prerequisite to ensure the application of LST products in various fields. Due to the influence of LST retrieval algorithms, atmospheric conditions, regional land cover types, topographic features, and climate change, the retrieval accuracy of different LST products varies in various regions [6].

Zhu et al. [1] summarized the index system and verification methods for ground verification of LST and emissivity, and analyzed the error sources of the verification process. Ma et al. [7] reviewed and compared four kinds of validation methods, and then some important issues in LST validation were discussed. Based on previous research, the most commonly used methods for LST accuracy assessment include the direct validation, cross-validation, the radiance-based validation, and the time series analysis.

The direct validation method compare the LST observed on the ground with the LST derived from sensors by time-space-angle matching. Cheng et al. [8] directly validated the FY-3D MERSI-II LST product using ground truth data from Wuhai experimental station and Surface Radiation Budget Network (SURFRAD), and results showed that the root-mean-square error (RMSE) of the LST retrieved by the split-window algorithm was between 1.6 K and 2.6 K, and the LST retrieval accuracy reached the expected target and had a high spatial resolution, which provides a basis for further development of LST retrieval algorithms and its applications in various research fields. Malakar et al. [9] performed direct validation of Landsat LST data with in situ observations from four SURFRAD sites and two inland water bodies (Salt Lake and Lake Tahoe) in the US, and results showed the usability of Landsat LST data for long-term monitoring of temperature trends, land cover, and land use change. Martin et al. [10] directly validated LST datasets

Manuscript received 15 June 2023; revised 21 September 2023; accepted 18 October 2023. Date of publication 23 October 2023; date of current version 6 November 2023. This work was supported in part by Fengyun Application Pioneering Project under Grant FY-APP-2022.0204 and in part by the Natural Science Foundation of China under Grant 42171101 and Grant 42271351. *(Corresponding author: Shanyou Zhu.)*

Yiyao Gao, Shanyou Zhu, and Yongming Xu are with the School of Remote Sensing and Geomatics Engineering, Nanjing University of Information Science and Technology, Nanjing 210044, China (e-mail: 20211248045@nuist.edu.cn; zsyzgx@163.com; xym30@nuist.edu.cn).

Guixin Zhang is with the School of Geographical Sciences, Nanjing University of Information Science and Technology, Nanjing 210044, China (e-mail: 001631@nuist.edu.cn).

Digital Object Identifier 10.1109/JSTARS.2023.3326956

© 2023 The Authors. This work is licensed under a Creative Commons Attribution-NonCommercial-NoDerivatives 4.0 License. For more information, see https://creativecommons.org/licenses/by-nc-nd/4.0/

obtained from several sensors, including Advanced Along-Track Scanning Radiometer, Geostationary Operational Environmental Satellites, moderate-resolution Imaging spectroradiometer (MODIS), and Spinning Enhanced Visible and Infrared Imager (SEVIRI) by spatially and temporally matching with LST data from global sites, results showed an average accuracy typically within ±2.0 K at night and ±4.0 K during the day. The direct validation method based on observed LST is simple and can directly evaluate the accuracy of remotely sensed LST, but the method requires the selection of a uniform subsurface for single or multipoint observations and relies on the accuracy of LST measurements as well as the ability to characterize surface heterogeneity at the image scale.

Cross-validation is the comparison of the LST inversion results to be examined with other LST products that have been validated with high accuracy. To test and quantify the temperature differences retrieved by different onboard sensors, a set of overlapping images was acquired and used for cross-validation. Preliminary statistical analysis showed a correlation between sensors in the test area and consistency in the mean values. Gao et al. [11] used the region of 31.671°N to 44.211°N and 10.739°W to 1.898°E as the study area, and performed cross-validation of FY-3C Visible and Infrared Radiometer LST with Terra/MODIS LST product. Silvestri et al. [12] cross-validated Advanced Spaceborne Thermal Emission and Reflection Radiometer data with Landsat 8 Thermal Infrared Sensor data in the thermal anomaly region. Trigo et al. [13] cross-validated the LST products from the SEVIRI image on the second generation Meteosat geostationary satellite with high-resolution AVHRR data for South America for the years 2015–2018. The average difference between the SEVIRI LST products is mostly within ±1°C, which meets the high accuracy criteria. Compared with the direct validation method, this method do not use ground truth measurements and, thus, is not limited by terrain and subsurface, but only the relative accuracy with respect to the reference LST products can be obtained, and the spatio-temporal normalization process between the data used for cross-validation will affect the accuracy assessment results to some extent.

The radiance-based validation method gives the accuracy of the land surface temperature (LST) product by comparing the retrieved LST with the adjusted and optimized LST by radiative transfer modeling. Given the atmospheric profile, the land surface emissivity and LST, the difference between the forward simulation radiance based on atmospheric radiative transfer models such as MODTRAN and the image radiance at the time of transit of the sensor is taken as the optimization target. The optimal value of LST is iteratively determined to ensure the minimum radiance difference by continually adjusting the LST inputted into the radiative transfer model. This method has the advantage of validating all-weather LST products, and avoids the direct measurement of surface temperature on the ground, which provides the possibility of evaluating the sensor retrieved LST on heterogeneous regions where field measurement LST are difficult to performed. So the radiance-based validation method is suitable for large-scale validation on a global scale. However, this method requires accurate land surface emissivity and the atmospheric profile data, as well as the accurate radiative transfer model, which might introduce additional errors in the validation process.

The time series based validation method first constructs long time series observations of relatively stable surface types (e.g., inland water bodies) [14] to obtain the background reference value, then it analyzes the time series stability and accuracy of the LST products according to the degree of their deviation from the background reference value. This method cannot obtain the absolute accuracy of the sensor retrieved LST, but it has the ability to detect observational anomalies of the on-orbit sensors due to factors such as cloud cover [15] or calibration drift [14], and it can also recalibrate radiance of the on-orbit thermal infrared sensors combined with field measurement data.

FY-4A satellite main load includes an advanced geostationary radiometer, interferometric atmospheric vertical sounder, lightning imager, and space environment monitoring instruments, which can monitor various meteorological elements, such as the atmosphere, clouds, surface, ocean, and space environment in real time. FY-4A AGRI scanning imaging radiometer has 14 channels, it can observe clouds, water vapor, vegetation, and surface, and it also has the ability to capture aerosols and snow and to clearly distinguish between different phases of clouds and high- and mid-level water vapor. The National Satellite Meteorological Center of China Meteorological Administration has released the FY-4A AGRI L2-level LST product, which has provided services for multiple fields, such as meteorology, resources, agriculture, and forestry. However, there are relatively few studies on how accurate the AGRI LST products are in different regions and at different times, and further evaluation work is needed. In this study, direct validation and cross-validation methods were conducted to evaluate the accuracy of FY-4A AGRI LST data by selecting the station-measured LST and the MODIS LST data at synchronization time, which can provide a reference role for the in-depth application of AGRI LST in more fields.

II. Data and Methods

A. Data

1) FY-4A ARGI Land Surface Temperature Products: FY-4A geostationary meteorological satellite, a new generation of Chinese geostationary orbiting meteorological satellites, was successfully launched on December 11, 2016, from the Xichang Satellite Launch Center by the Long March 3B rocket. From May 8, 2018, users in China and the Asia-Pacific region can officially receive data from FY-4A. The imager acquires 40 full-disc cloud maps and 165 Chinese regional cloud maps daily, with Chinese regional observations ranging from 3°–55°N and 60°–137°E.

The real-time LST products provided by FY-4A AGRI include both Chinese regional/nominal and full-disc/nominal products, which have been released to the public by the Feng Yun Satellite Remote Sensing Data Network (https://satellite.nsmc.org.cn/portalsite/default.aspx). The AGRI LST is retrieved from two thermal infrared channels by using the split-window algorithm. The coefficients of the split-window algorithm are determined by the least squares simulation method based on thermal infrared radiance simulated from the radiative

transfer model MODTRAN. In order to cross-validate with the MODIS land surface temperature at the synchronous moment, and considering the missing data in some angle files, a total of 38 sets of AGRI LST products at 11:00 A.M. and 22:00 P.M. of Beijing Time for every 16 days from January 3 to December 21, 2021, have been selected for this study.

AGRI LST has a spatial resolution of 4 km in NetCDF format, the longitude of the subsatellite point of 104.7°E. This study also uses the FY-4A L1 GEO data, which is the 4 km positioning information obtained from the multichannel scanning radiometer data after geolocation processing. The nominal satellite zenith data (NOMSatelliteZenith), nominal satellite azimuth data (NOMSatelliteAzimuth), nominal solar zenith data (NOMSunZenith), and nominal solar azimuth data (NOMSunAzimuth) in the GEO dataset are also used. Due to the distorted images cause difficulties in quantitative analysis and position alignment, full-disk 4 km GEO data was used to construct a latitude and longitude lookup table to reproject the disk data to equal latitude and longitude projection, and then batch geometric correction of the AGRI LST data were performed.

2) Land Surface Temperature Observation Data: Ground-based observations are the basis for direct accuracy assessment of LST products. Meteorological station observations are one of the most commonly used data, which provide high-quality, high temporal resolution of land surface temperature, air temperature, visibility, radiation, humidity, and other meteorological elements. Chinese national meteorological stations are located in 12 temperature zones, 24 wet and dry zones, and 6 climate zones [16], [17]. Stations are located in places that can better respond to the characteristics of a larger range of local geographic elements, shallow mountainous, and hilly areas. The station site is selected in the top of a relatively flat mountain, the desert Gobi, grasslands, and forested areas, and other single-geomorphic site is generally located in response of the natural conditions of the local subsurface with a good representation. Chinese meteorological stations mainly use platinum resistance temperature sensors to measure LST. According to the specification for surface meteorological observations, when LST observations are carried out, platinum resistance temperature sensors must be placed horizontally on the surface of the ground, with the temperature-sensing portion generally buried in the soil and the other portions exposed to the air. The data are automatically transmitted from each station to the National Meteorological Information Center of China Meteorological Administration and released to the public through appropriate channels.

In this study, the ground LST observations of 2454 stations across China were selected to verify the FY-4A AGRI LST accuracy. The temporal resolution of LST observation is 10 min. The ground LST measured on January, April, July, and October of 2021 with a quality control code of 0 (no data anomaly is found through quality control, or the data are anomalous but the data are finally confirmed to be correct) is chosen.

3) MODIS Data: The MODIS data included a total of 38 sets of daily land surface temperature products (MOD11A1) imaged at 11 A.M. and 22 P.M. of Beijing Time every 16 days from January 3 to December 21, 2021, the geolocation product (MOD03) and the global land cover product of 2021 (MCD12Q1), with spatial resolutions of 1 km, 1 km, and 500 m, respectively. The LST_Day_1 km, LST_Night_1 km, QC_Day, QC_Night, Day_view_time, Night_view_time data in the MOD11A1 LST product dataset, and the Sensor Zenith, Sensor Azimuth, Solar Zenith, Solar Azimuth data in the MOD03 dataset were used in cross-validation. Due to the presence of clouds and other interfering factors, the quality of every image element in the MODIS product is not always reliable, so quality control files are provided in the product describing the level of confidence. When using MODIS LST to participate in cross-validation, LST image with quality values of 0 and 1 in the LST quality control file were selected (representing LST error less than 1 K and less than 2 K, respectively).

Considering the completeness of the required data of satellite observation angles and the synchronous solar angles, MOD11A1 data used for LST cross-validation are located in the region of 36°13′N-39°57′N, 101°49′E-106°29E, as illustrated in Fig. 1. According to the 17 land cover categories defined by the IGBP Global Vegetation Classification Scheme, the MCD12Q1 dataset of the experiment area contains twelve land cover types, that are evergreen needleleaf forests, deciduous broadleaf forests, mixed forests (MF), open shrublands, woody savannas (WSA), savannas, Grasslands (GRA), permanent wetlands (WET), croplands (CRO), urban and built-up lands (URB), barren sparse vegetation (BSV), and water bodies. In the experiment region, the top three land cover types are BSV, GRA, and CRO. MODIS data are raster data organized in a tessellated manner, and the projection is a sinusoidal projection. The coordinates need to be uniformly converted to the WGS84 coordinate system, and geometric correction was performed. Since the spatial resolution of the MODIS daily LST product and geolocation product is 1 km, the aggregated averaging method was used to unify the spatial resolution of MODIS data to 4 km.

B. Direct Verification Method

In this article, ground temperature data are linearly interpolated based on the satellite transit time to obtain measurements corresponding to the imaging time, and the field stations located on the AGRI image are found based on geometric matching by using the geographical position of these two kinds of data. When there is only one station observation data in the AGRI pixel [18], the station LST is used as the contrast value to directly verify the accuracy of the LST product. While if there are multiple stations located within one AGRI pixel, the grid value of AGRI LST is compared with the arithmetic mean value of these stations. Four indicators, namely, the correlation coefficient, mean absolute error (MAE), RMSE, and mean bias error (MBE) are used to evaluate the AGRI LST accuracy.

C. Cross-Validation Method

For cross-validation, the differences between the two datasets need to be considered, and the temporal, spatial, and angular matching process of the two datasets need to be performed. The cross-validation study was carried out by selecting a common area, and the FY-4A AGRI LST have no missing values and imaged within 5 min before and after the observation of the

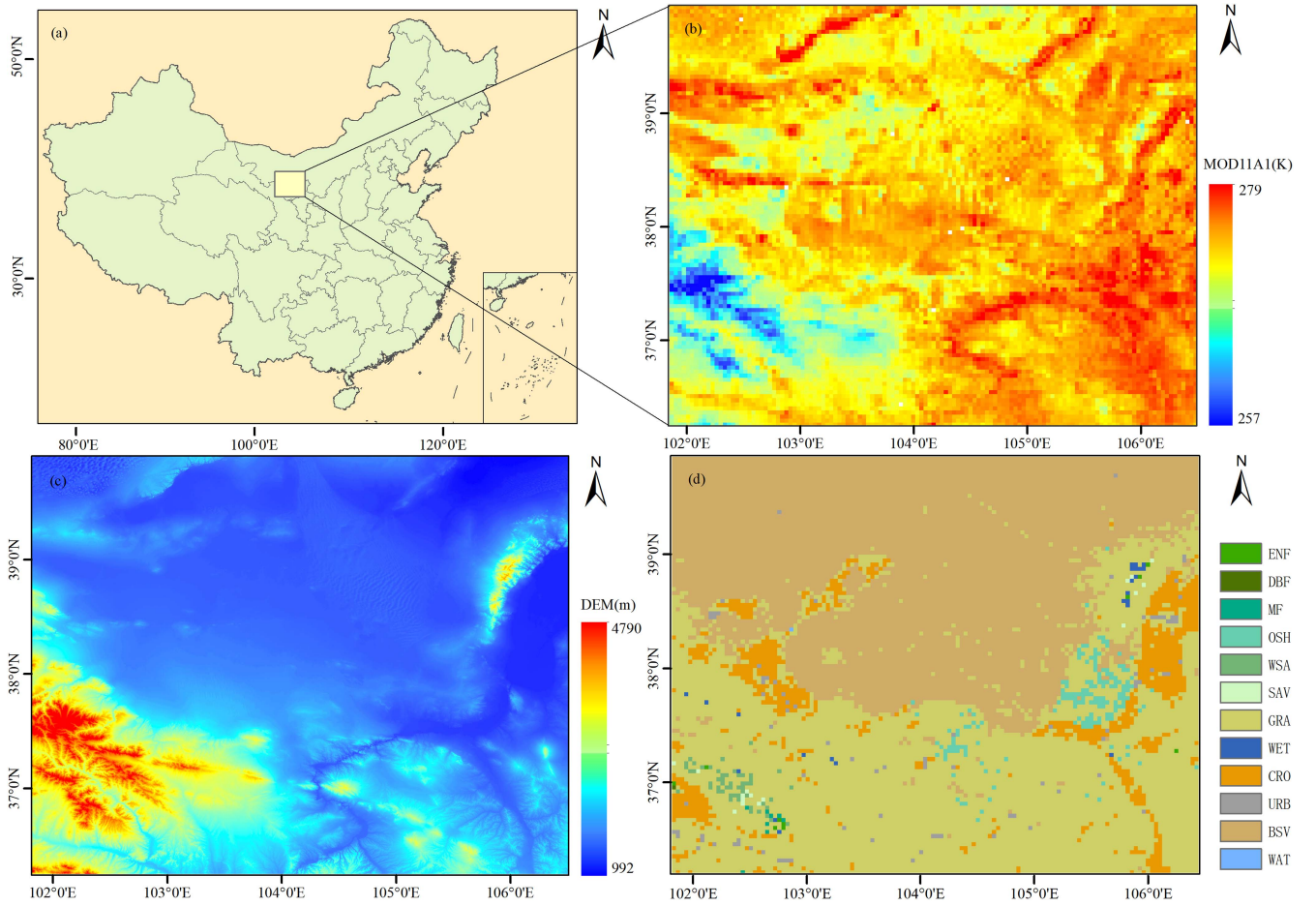

Fig. 1. Cross-validation experiment area and corresponding data. (a) Location of the experiment area. (b) MODIS LST at 22:00 on November 3, 2021. (c) DEM distribution. (d) Land use types distribution.

MOD11A1 LST. Rasmussen et al. [19] investigated the differences in LST due to angle differences at a specific savanna site in West Africa by building a geometric-optical model and extended the results to areas with denser canopy cover. The results showed that the effect of angle on LST is greater than 1 °C and varies seasonally when two sensors are cross-validated for LST. To reduce the effect of angle on LST cross-validation, the kernel method (kernel model) proposed in [20] was used to correct the angle influence on the FY-4A AGRI LST.

The main principles and processes of the angle correction kernel model are briefly described as follows.

Statistical methods show that the dependence of LST on the observation angle and solar angle can be expressed as

$$\frac{T\left(\theta_v,\theta_i,\Delta\varphi\right)}{T_0} = 1 + A\Phi\left(\theta_{\mathrm{v}}\right) + D\Psi\left(\theta_v,\theta_i,\Delta\varphi\right) \tag{1}$$

where θ_v, θ_i, and $\Delta\varphi$ are the satellite zenith angle, the solar zenith angle, and the sun-satellite relative azimuth angle, respectively; T_0 is the LST when the observed zenith angle is 0, A, and D are coefficients estimated from the satellite observations; $\Phi(\theta_v)$ is the "emissivity kernel"; $\Psi(\theta_v,\theta_i,\Delta\varphi)$ is the "solar kernel," which can be calculated by

$$\Phi\ \left(\theta_v\right) = 1 - \cos\left(\theta_v\right) \tag{2}$$

$$\Psi\ \left(\theta_v,\theta_i,\Delta\varphi\right) = \sin\left(\theta_v\right)\cos\left(\theta_i\right)\sin\left(\theta_i\right)\cos\left(\theta_i-\theta_v\right)\cos\left(\Delta\varphi\right). \tag{3}$$

The emissivity kernel is only related to the variation in the observed zenith angle. As complex land surface, the emissivity kernel is based on the assumption that the surface emissivity changes significantly from the subsurface point to a larger observational zenith angle (e.g., greater than 40°). Many features have a small change in emissivity with the observed zenith angle, and bare earth emissivity typically decreases with increasing observed zenith angle. A decrease in emissivity with increasing zenith angle will result in a larger LST retrieval error, with a negative value of A in (1). The "solar core" simulates the effect of shadows and sunlight irradiation on the different surface nonuniform heating in the field of view of the sensor, which is related to the observation angle and solar angle.

Because LST is usually observed for nonsubsurface points, according to (1), LST relationship at two different observation times and observation angles can be expressed as

$$\frac{T_1}{T_2} = \frac{1 + A\Phi_1 + D\Psi_1}{1 + A\Phi_2 + D\Psi_2}. \tag{4}$$

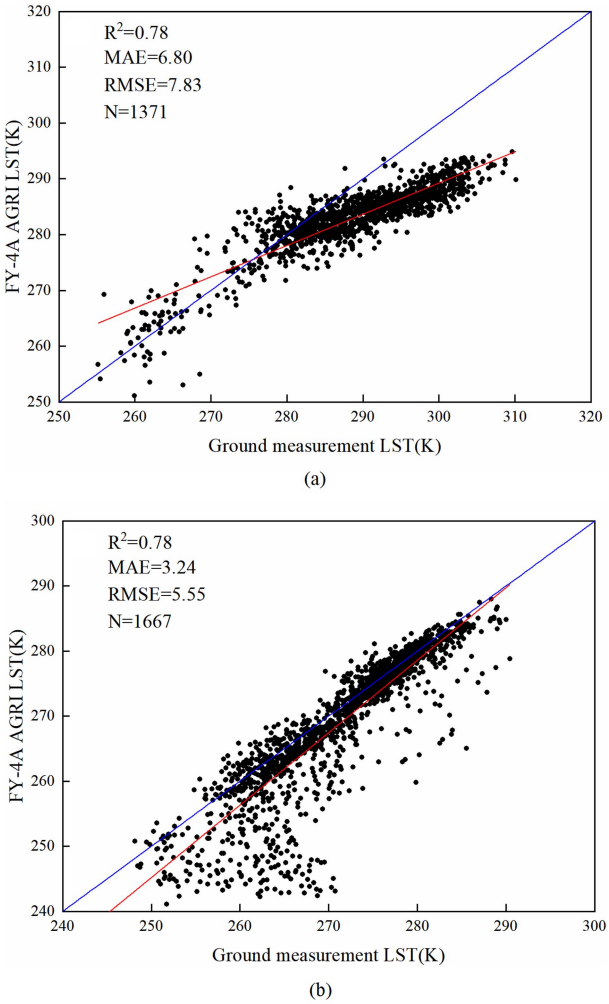

Fig. 2. Scatterplot of ground-measured site temperature compared with FY-4A LST. (a) Comparison scatterplot at 11:00 on January 19, 2021. (b) Comparison scatterplot at 22:00 on January 19, 2021.

For the correction of the angle difference of LST observations, synchronous, or quasi-synchronous data of nighttime observations can be selected. Because the nighttime moment $\Psi = 0$, (4) can be converted to (5). Φ_1 and Φ_2 can be determined based on (2) by using the zenith angles observed by both sensors, and parameter A is then calculated from (5) by inputting the nighttime LST T_{n1} and T_{n2} of each sensor

$$T_{n1} - T_{n2} = A\left(\Phi_1 T_{n2} - \Phi_2 T_{n1}\right). \tag{5}$$

And then, parameter D can be calculated using (6) according to the simultaneous LST data T_{d1} and T_{d2} observed by both sensors

$$D = \frac{T_{d1} - T_{d2} - A\left(\Phi_1 T_{d2} - \Phi_2 T_{d1}\right)}{\left(\Psi_1 T_{d2} - \Psi_2 T_{d1}\right)}. \tag{6}$$

Once the parameters A and D are determined, the angle-corrected LST T can be obtained by (1). In the case of higher observed zenith angles (e.g., greater than 50°), the thermal infrared sensor retrieved LST has a large uncertainty, and these observations should not be substituted into (5) and (6) for the calculation of parameters A and D.

TABLE I
ACCURACY EVALUATION RESULTS OF THE DIRECT VERIFICATION METHOD

Date	Correlation coefficient	MAE (K)	RMSE (K)
January 3, 11:00	0.92	6.99	8.34
January 3, 22:00	0.88	3.63	5.79
January 19, 11:00	0.89	6.80	7.89
January 19, 22:00	0.88	3.24	5.55
April 9, 11:00	0.68	8.76	9.78
April 9, 22:00	0.86	2.96	4.14
April 25, 11:00	0.82	11.23	12.75
April 25, 22:00	0.83	5.48	6.99
July 14, 11:00	0.54	14.87	16.19
July 14, 22:00	0.81	5.51	6.06
July 30, 11:00	0.56	14.57	15.73
July 30, 22:00	0.80	4.82	5.68
October 2, 11:00	0.80	10.84	12.17
October 2, 22:00	0.92	4.61	5.22
October 18, 11:00	0.78	5.76	6.81
October 18, 22:00	0.85	3.62	5.19

Furthermore, Fig. 2 gives a scatter plot between the ground truth site temperature and the FY-4A AGRI LST for two instances on January 19, it presents a more visual comparison and can be used to analyze the relationship between two kinds of data to verify the accuracy of the AGRI LST.

Finally, the accuracy of the cross-validation was evaluated using the error evaluation indicators.

III. Results and Analysis

A. Results of Direct Verification Method

To match the MODIS data dates in the cross-validation, the ground truth data with the dates shown in Table I were selected for direct validation of the AGRI LST for 16 instances in 2021. According to Table I, the mean value of the correlation coefficient between the ground measurement LST and the FY-4A AGRI LST is 0.80, the MAE is 7.1 K, the RMSE is 8.39 K, and the MBE is 6.04 K, which means the FY-4A AGRI LST is underestimated by about 6 K on average. In terms of diurnal distribution, the nighttime AGRI LST product is closer to the site truth data, and the correlation between them is 0.85, and the MAE and RMSE of the AGRI LST is 4.23 K and 5.58 K, respectively.

Table II shows the comparison of land surface temperature accuracy in different seasons, which indicates the FY-4A AGRI LST products in winter are closest to the measured values at the site, followed by autumn, and summer has the biggest MAE and RMSE. In northern China, the vegetation cover is relatively

TABLE II
COMPARISON OF ACCURACY IN DIFFERENT SEASONS

Season (Month)	Correlation coefficient	MAE (K)	RMSE(K)
Spring (April)	0.80	7.11	8.42
Summer (July)	0.68	9.94	10.92
Autumn (October)	0.84	6.21	7.35
Winter (January)	0.89	5.16	6.89

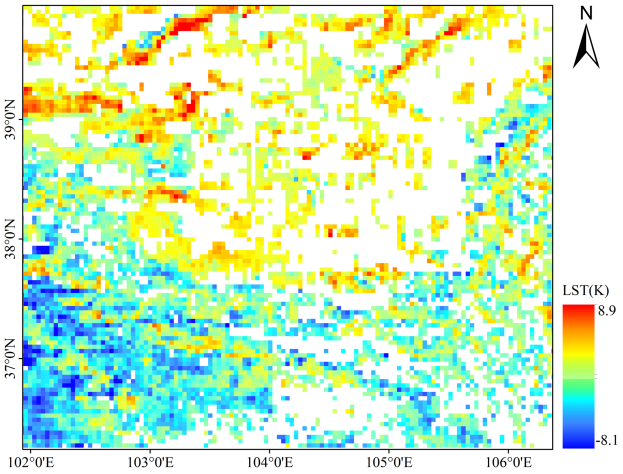

Fig. 3. Spatial distribution of cross-validation errors at 22:00 of Beijing Time on January 19, 2021.

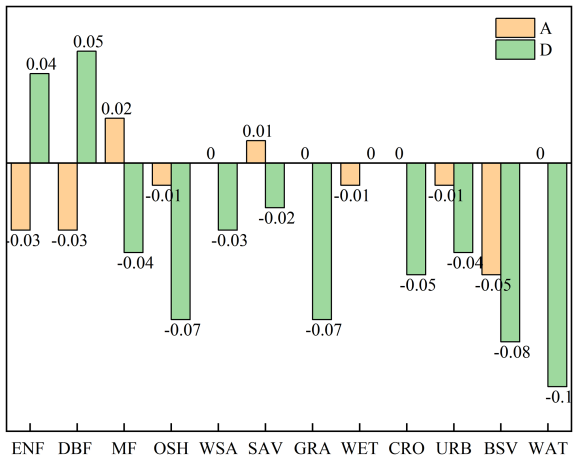

Fig. 4. Average values of parameters A and D for different land use types.

lower in autumn and winter due to the seasonal influence, so the spatial heterogeneity of a certain area around the measured site is smaller, and the spatial representativeness of the measured LST at the site is better. Moreover, the cloud amount is usually smaller in autumn and winter and it has fewer influence on satellite imaging, so there are little missing data for AGRI LST products.

By analyzing the spatial distribution characteristics of FY-4A AGRI LST products, in general, the satellite derived LST are consistent with the station measured LST. The areas with better AGRI LST accuracy are mostly concentrated in Hainan and Guangxi of southern China, and in Xinjiang and Tibet of western China, where have a relatively homogeneous land surface type, corresponding to the spatial heterogeneity within the AGRI pixels. The AGRI LST precision in Fujian, Zhejiang, and Jiangsu of the east coast and in Sichuan, Chongqing, Guizhou, Hunan, and Hubei of the central China are relatively poor, mainly due to the combination influence of local heterogeneous surface cover and atmospheric conditions such as frequently occurring overcast and rain. It is found that the land surface covered with lower vegetation is more prone to drastic temperature changes, while the surface with high vegetation cover has larger heat capacity and thermal inertia, and the warming process is more slower. Cheng et al. [8] used the Wuhai experimental station to validate the LST products of Fengyun satellite in southwestern Inner Mongolia and found that the dry surface is more sensitive to surface emissivity compared to the wet surface, and LST with large errors are mainly distributed in sparse shrubland and bare ground areas. Gao [21], similarly, evaluated microwave global LST products from the Fengyun-3C satellite and summarized similar conclusions, and LSTs were underestimated to a greater extent for desert and sparse vegetation, depression, and sparse scrub and to a lesser extent for woodlands such as deciduous coniferous and evergreen broadleaf forests.

The reasons for the mean absolute error and RMSE are, on the one hand, the low signal-to-noise ratio of the Fengyun satellite data itself [22], which leads to its low LST retrieval accuracy, and the accuracy is also affected by the uncertainty of the land surface emissivity and atmospheric water vapor content. On the other hand, because the spatial resolution of the satellite data is 4 km, the actual measured value of the site is point to point, the ground instrument observation scale is mostly a single type of homogeneous surface, while the image metric scale usually covers not less than one surface type, which brings great uncertainty and error for the nonuniform subsurface. That means the ideal ground temperature validation site should be homogeneous ground with less spatial heterogeneity [23].

The spatial heterogeneity of LST is often more pronounced in daytime than in nighttime due to the surface heterogeneity, the warming effect of different components, and the temperature difference between light and shadow components affected by solar irradiation angle [24], [25]. It has been noted that LST differences between different land cover types may reach 10 K on a spatial scale of less than a few centimeters [26], while LSTs in the same region can vary by more than 1 K within one minute [27].

Considering the research can only collect field observation LST data on January, April, July, and October, and need to consider MODIS imaging time to perform cross-validation, only 16 moments of AGRI LSTs were selected to participate in the direct validation. While these data are generally representative of the daytime and nighttime conditions in different seasons, the validation results might have some suspicious. If more station observations were obtained, the accuracy of AGRI LST can be further analyzed by the direct validation method to make the conclusions more reliable.

TABLE III
COMPARISON OF ACCURACY BEFORE AND AFTER ANGLE CORRECTION FOR DIFFERENT DATE

Date	Correlation coefficient (before correction)	RMSE(K) (before correction)	Correlation coefficient (after correction)	RMSE(K) (after correction)
January 3, 11:00	0.54	4.71	0.69	1.44
January 3, 22:00	0.70	2.31	0.74	1.20
January 19, 11:00	0.31	6.15	0.77	1.51
January 19, 22:00	0.68	1.97	0.69	1.16
February 4, 11:00	0.16	3.84	0.67	0.85
February 4, 22:00	0.69	4.55	0.97	4.46
February 20, 11:00	0.64	4.52	0.73	0.75
February 20, 22:00	0.84	4.60	0.96	2.01
March 8, 11:00	0.82	6.73	0.98	1.47
March 8, 22:00	0.75	3.53	0.88	2.94
March 24, 11:00	0.79	10.26	0.99	0.83
March 24, 22:00	0.41	4.04	0.96	1.44
April 9, 11:00	0.47	9.81	1.00	0.29
April 9, 22:00	0.25	3.54	0.55	1.93
May 11, 11:00	0.78	8.89	0.97	2.53
May 11, 22:00	0.77	3.70	0.87	3.03
May 27, 11:00	0.70	7.67	0.86	3.27
May 27, 22:00	0.57	4.02	0.75	3.93
June 12, 11:00	0.96	6.76	0.96	4.28
June 28, 11:00	0.88	10.25	0.91	6.47
July 14, 11:00	0.79	6.94	0.98	1.33
July 14, 22:00	0.36	4.17	0.78	3.16
July 30, 11:00	0.90	10.36	0.97	3.14
July 30, 22:00	0.88	3.24	0.91	4.71
August 15, 11:00	0.86	9.79	0.99	1.31
August 15, 22:00	0.01	7.24	0.89	2.10
August 31, 11:00	0.79	4.38	0.99	0.98
August 31, 22:00	0.45	5.08	0.96	2.38
September 16, 11:00	0.61	7.43	0.98	2.41
September 16, 22:00	0.90	4.45	0.98	3.15
October 2, 11:00	0.71	5.49	0.99	0.95
October 2, 22:00	0.78	3.87	0.96	2.13
November 3, 11:00	0.72	5.56	0.99	1.11
November 3, 22:00	0.71	2.18	0.96	1.03
December 5, 11:00	0.31	5.22	0.97	1.12
December 5, 22:00	0.64	2.37	0.94	1.18
December 21, 11:00	0.46	5.12	0.93	1.33
December 21, 22:00	0.68	2.30	0.96	1.37
Average value	0.64	5.45	0.90	2.12

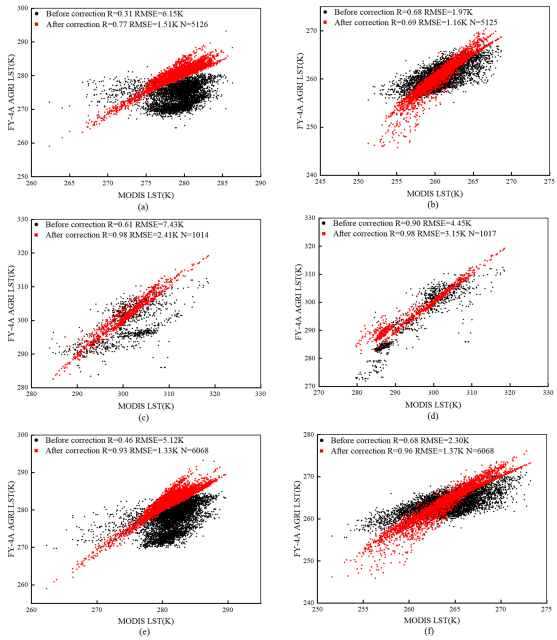

Fig. 5. Scatter plot of FY-4A LST before and after angle correction and MOD11A1 LST. (a) Comparison scatterplot at 11:00 on January 19. (b) Comparison scatterplot at 22:00 on January 19. (c) Comparison scatterplot at 11:00 on September 16. (d) Comparison scatter plot at 22:00 on September 16. (e) Comparison scatterplot at 11:00 on December 21. (f) Comparison scatterplot at 22:00 on December 21.

B. Results of Cross-Validation Method

The LST products after cloud masking and quality control have some missing data due to clouds, fog, rain, snow, and other weather disturbances, and the dates with missing value points greater than 80% are not involved in the cross-validation process. For RMSE and MAE reflect the same error trend and pattern based on the result of direct validation, so RMSE was chosen to carry out the subsequent analysis of the AGRI LST error.

The cross-validation results show that the average correlation coefficient between the two LSTs is 0.64, the spatial and temporal distribution trends are consistent, and the RMSE of the AGRI LST is 5.45 K, which has reasonable accuracy. Compared to the MOD11A1 LST product, the AGRI LST product appears to be underestimated. The nighttime assessment is better than the daytime assessment, especially in terms of the RMSE, with an average RMSE of 7.10 K during the daytime and 4.00 K at night. This is because there is less water vapor in the atmosphere and no influence of solar irradiation, and the land surface behaves almost uniformly at night. This is in agreement with the results of Guillevic et al. [28].

Taking the cross-validation error at 22:00 of Beijing Time on January 19, 2021 as an example, the spatial distribution of LST difference between MODIS and AGRI is given in Fig. 3. Based on Fig. 3, the maximum LST difference is 8.8 K, and RMSE is 1.97 K. According to Figs. 1 and 3, it can be found that AGRI LST has larger underestimation in BSV and CRO covered regions, while AGRI LST is higher than MODIS LST where are covered with GRA type. Moreover, AGRI LST is overestimated at the southwest region with higher altitude. The error distribution in Fig. 3 illustrates that land cover types and

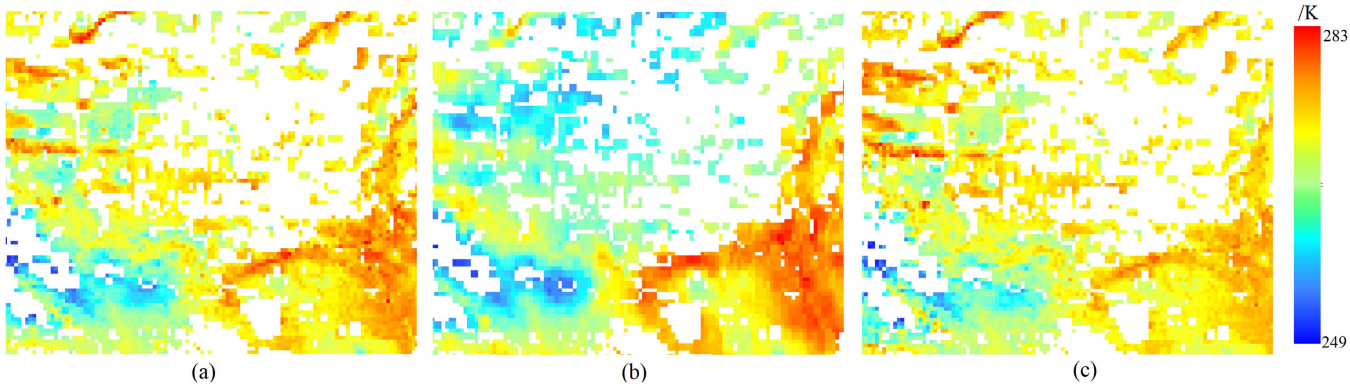

Fig. 6. Spatial distribution of FY-4A AGRI LST before and after angle correction, compared with MOD11A1 LST at 22:00 on November 3. (a) MOD11A1 LST. (b) AGRI LST before angle correction. (c) AGRI LST after angle correction.

the topography have large effect on LST distribution and LST retrieval algorithm from different sensors.

Remotely sensed LST is related to directionality [29], and due to the high spatial heterogeneity of the surface, this directionality may lead to significant differences between LST products obtained over the same area and observation time but at different observation angles [30], [31]. When cross-validating LST products derived by different sensors, the differences in observation angles of various satellite sensors need to be taken into account.

According to (1)–(6), the angle correction parameters A and D were determined to correct the angle influence on AGRI LST. Combined with the MCD12Q1 global land use type products in the study area, Fig. 4 illustrates that the average parameters A and D in the angle correction are influenced by the land use types.

According to Fig. 4, the absolute value of parameter A mostly tends to be 0. The maximum value appears in the MF, the minimum value is in the BSV, GRA, WSA, and CRO are closer. This may be related to the dependence of the emissivity on the viewpoint, where a negative value of A is consistent with a decrease in the emissivity with the viewpoint. For surfaces with uniform bare ground, the emissivity decreases with increasing zenith angle, but for other surfaces, such as grasslands, this change is expected to be negligible. The parameter D is strongly influenced by the tree cover on the land and is positively correlated with it, with high values of D in areas with tall trees, with maximum values occurring in broadleaf forest areas and low values in water and bare ground areas. Similar conclusion was reached in [20] when cross-validating MODIS and SEVIRI LST products in Mediterranean Europe and North Africa.

The cross-validation results between the research selected FY-4A AGRI LST before and after angle correction and the MOD11A1 LST product are shown in Table III.

According to Table III, the differences between AGRI LST and MODIS LST decrease for all dates, the average correlation coefficient increased to 0.90 after angle correction, and the RMSE decreased to 2.12 K. The maximum and minimum RMSE after angle correction is 6.47 K and 0.29 K, respectively. The average correlation coefficient before and after angle correction at daytime increased from 0.66 to 0.92, and the RMSE decreased from 6.99 K to 1.87 K, while the average RMSE at night only decreased by 1.32 K. This is due to the fact that during the daytime, the directionality of the solar irradiation with various solar zenith and azimuth angles results in a mix of shaded and illuminated surfaces that imaged by AGRI sensor at different observation angles, whereas at night there are no solar irradiation.

TABLE IV
COMPARISON OF ANGLE CORRECTION EFFECTS IN DIFFERENT SEASONS

Season (Month)	Correlation coefficient (before correction)	RMSE (K) (before correction)	Correlation coefficient (after correction)	RMSE (K) (after correction)
Spring (March-May)	0.63	6.22	0.88	2.16
Summer (June-August)	0.69	6.82	0.93	2.99
Autumn(September-November)	0.74	4.83	0.98	1.80
Winter (December-February)	0.55	3.97	0.84	1.53

The cross-validation results before and after the angle correction for different seasons are tabulated in Table IV. According to Table IV, there are some differences in the angle correction effect in different seasons. The largest RMSE after angle correction decreases by 4.06 K in Spring, followed by 3.83 K, 3.03 K, and 2.44 K in summer, autumn, and winter, respectively.

Taking some random moments as the example, Fig. 5 shows the cross-validation scatter plots of the FY-4A AGRI LST before and after angle correction with the MOD11A1 LST. From Fig. 5, the correlation coefficients increase and RMSEs decrease a lot for all data.

Moreover, the spatial distributions of FY-4A AGRI LST before and after angle correction compared with MOD11A1 LST at 22:00 on November 3, 2021 are illustrated in Fig. 6. Before angle correction, there is large difference between AGRI LST

[see Fig. 6(b)] and MODIS LST [see Fig. 6(a)], especially at regions with the land use type of BSV. Compared Fig. 6(a) with Fig. 6(c), the LST spatial distribution characteristics of these two LSTs are more consistent after angle correction. The maximum, minimum, mean, and standard deviation of the LST before AGRI angle correction are 276.39 K, 262.73 K, 271.90 K, and 2.61 K, respectively, while the values change to 283.02 K, 249.83 K, 273.28 K, and 3.21 K after correction, which are closer to the MODIS LST image statistics of 279.78 K, 256.00 K, 272.78 K, and 3.07 K. LST in the area with sparse vegetation cover and large topographic relief had a larger error due to the angle difference between two sensors.

IV. Conclusion

In this article, the direct validation method and the cross-validation method were used to carry out accuracy assessment on ARGI LST products to evaluate the accuracy and the usability of LST products in different regions, seasons, and land use types. Based on the processing of spatio-temporal normalization, the angle correction model is applied to the ARGI LST products to improve the reliability of the ARGI LST product evaluation.

The accuracy of the FY-4A AGRI LST products is high. Through the time series analysis of the ARGI LST products compared with field measurement LST, it is found that they can reflect the LST trends more accurately in terms of daily and seasonal changes. The spatial distribution analysis of the ARGI LST products revealed that the accuracy was lower in areas with small vegetation cover, while the LST underestimation of was smaller in areas with higher vegetation cover, such as deciduous coniferous forests, evergreen broad-leaved forests, and other woodlands.

Using the more mature MOD11A1 daily LST product cross-validated with the FY-4A AGRI LST product, the validation results show that the correlation between the two datasets is high and that the error produced by the algorithm is within acceptable limits. The angle correction model was then applied to the AGRI LST product, and the results indicate that the average correlation between the corrected MOD11A1 product and the ARGI LST product improved from 0.64 to 0.90, and the RMSE decreased from 5.45 K to 2.21 K. The angle effect on LST of the two sensors was well reduced, and the accuracy and reliability of the ARGI LST product was improved.

There are still some shortcomings in the accuracy assessment of the FY-4A AGRI LST products that need to be further addressed. The direct validation method compares point-by-point filed measurement with satellite grid LST corresponding to multiple land use types, the errors caused by station representativeness and subsurface heterogeneity still need to be further investigated. In addition, the cross-validation can also be verified by comparison with other internationally recognized satellite LST products with high quality.

Acknowledgment

The authors would like to thank the National Aeronautics and Space Administration for providing the MODIS data and also like to thank the Fengyun Satellite Remote Sensing Data Service Network for providing FY-4A AGRI land surface temperature data as well as geographic information data.

References

[1] J. S. Zhu et al., "Ground validation of land surface temperature and surface emissivity from thermal infrared remote sensing data," *Nat. Remote Sens. Bull.*, vol. 25, no. 8, pp. 1538–1566, 2021, doi: 10.11834/jrs.20211299.

[2] B. Bayat et al., "Toward operational validation systems for global satellite-based terrestrial essential climate variables," *Int. J. Appl. Earth Observation Geoinformation*, vol. 95, Mar. 2021, Art. no. 102240, doi: 10.1016/j.jag.2020.102240.

[3] Z. L. Li et al., "Satellite-derived land surface temperature: Current status and perspectives," *Remote Sens. Environ.*, vol. 131, pp. 14–37, Apr. 2013, doi: 10.1016/j.rse.2012.12.008.

[4] M. C. Anderson, R. G. Allen, A. Morse, and W. P. Kustas, "Use of Landsat thermal imagery in monitoring evapotranspiration and managing water resources," *Remote Sens. Environ.*, vol. 122, pp. 50–65, Jul. 2012, doi: 10.1016/j.rse.2011.08.025.

[5] A. Mokhtari et al., "Calculating potential evapotranspiration and single crop coefficient based on energy balance equation using Landsat 8 and Sentinel-2," *ISPRS J. Photogrammetry Remote Sens.*, vol. 154, pp. 231–245, Aug. 2019, doi: 10.1016/j.isprsjprs.2019.06.011.

[6] X. C. Meng, H. Li, Y. M. Du, B. Cao, Q. H. Liu, and B. Li, "Retrieval and validation of the land surface temperature derived from Landsat 8 data: A case study of the Heihe river basin," *J. Remote Sens.*, vol. 22, no. 5, pp. 857–871, 2018, doi: 10.11834/jrs.20187411.

[7] J. Ma, J. Zhou, S. M. Liu, and Y. J. Yu, "Review on validation of remotely sensed land surface temperature," *Adv. Earth Sci.*, vol. 32, no. 6, pp. 615–629, 2017.

[8] Y. L. Cheng, H. Wu, Z. L. Li, and Y. G. Qian, "Retrieval and validation of the land surface temperature from FY- 3D MERSI-II," *Nat. Remote Sens. Bull.*, vol. 25, no. 8, pp. 1792–1807, 2021, doi: 10.11834/jrs.20211302.

[9] N. K. Malakar, G. C. Hulley, S. J. Hook, K. Laraby, M. Cook, and J. R. Schott, "An operational land surface temperature product for Landsat thermal data: Methodology and validation," *IEEE Trans. Geosci. Remote Sens.*, vol. 56, no. 10, pp. 5717–5735, Oct. 2018, doi: 10.1109/TGRS.2018.2824828.

[10] M. A. Martin, D. Ghent, A. C. Pires, F. - M. Göttsche, J. Cermak, and J. J. Remedios, "Comprehensive in situ validation of five satellite land surface temperature data sets over multiple stations and years," *Remote Sens.*, vol. 11, no. 5, Jan. 2019, Art. no. 479, doi: 10.3390/rs11050479.

[11] C. Gao et al., "Land surface temperature retrieval from FY-3C/VIRR data and its cross-validation with Terra/MODIS," *IEEE J. Sel. Topics Appl. Earth Observ. Remote Sens.*, vol. 10, no. 11, pp. 4944–4953, Nov. 2017, doi: 10.1109/JSTARS.2017.2728082.

[12] M. Silvestri, V. Romaniello, S. Hook, M. Musacchio, S. Teggi, and M. F. Buongiorno, "First comparisons of surface temperature estimations between ECOSTRESS, ASTER and Landsat 8 over Italian volcanic and geothermal areas," *Remote Sens.*, vol. 12, no. 1, Jan. 2020, Art. no. 458, doi: 10.3390/rs12010184.

[13] I. F. Trigo, S. L. Ermida, J. P. A. Martins, C. M. Gouveia, F. - M. Göttsche, and S. C. Freitas, "Validation and consistency assessment of land surface temperature from geostationary and polar orbit platforms: SEVIRI/MSG and AVHRR/Metop," *ISPRS J. Photogrammetry Remote Sens.*, vol. 175, pp. 282–297, May 2021, doi: 10.1016/j.isprsjprs.2021.03.013.

[14] S. J. Hook, R. G. Vaughan, H. Tonooka, and S. G. Schladow, "Absolute radiometric in-flight validation of mid infrared and thermal infrared data from ASTER and MODIS on the Terra spacecraft using the Lake Tahoe, CA/NV, USA, automated validation site," *IEEE Trans. Geosci. Remote Sens.*, vol. 45, no. 6, pp. 1798–1807, Jun. 2007, doi: 10.1109/TGRS.2007.894564.

[15] C. J. Merchant et al., "The surface temperatures of Earth: Steps towards integrated understanding of variability and change," *Geoscientific Instrum. Methods Data Syst.*, vol. 2, no. 2, pp. 305–321, Dec. 2013, doi: 10.5194/gi-2-305-2013.

[16] J. Y. Zheng, J. J. Bian, Q. S. Ge, Z. X. Hao, Y. H. Yin, and Y. M. Liao, "The climate regionalization in China for 1981–2010," *Chin. Sci. Bull.*, vol. 58, no. 30, pp. 3088–3099, 2013.

[17] J. Y. Zheng, J. J. Bian, Q. S. Ge, and Y. H. Yin, "The climate regionalization in China for 1951-1980 and 1981-2010," *Geographical Res.*, vol. 32, no. 6, pp. 987–997, 2013.

[18] B. D. Xu, J. Li, Q. H. Liu, X. Z. Xin, Y. L. Zeng, and G. F. Yin, "Review of methods for evaluating representativeness of ground station observations," *J. Remote Sens.*, vol. 19, no. 5, pp. 703–718, Jun. 2021, doi: 10.11834/jrs.20154178.

[19] M. O. Rasmussen, F. M. Gottsche, F. - S. Olesen, and I. Sandholt, "Directional effects on land surface temperature estimation from Meteosat second generation for Savanna landscapes," *IEEE Trans. Geosci. Remote Sens.*, vol. 49, no. 11, pp. 4458–4468, Nov. 2011, doi: 10.1109/TGRS.2011.2144604.
[20] K. Y. Vinnikov et al., "Angular anisotropy of satellite observations of land surface temperature," *Geophysical Res. Lett.*, vol. 39, no. 23, 2012, Art. no. 112361, doi: 10.1029/2012GL054059.
[21] H. Gao, R. H. Xu, and S. L. Wu, "Accuracy evaluation of the FengYun-3C global land surface temperature products retrieval from microwave radiation imager," *Geoscientific Instrum. Methods Data Syst.*, vol. 41, no. 4, pp. 1–8, 2018, doi: 10.16765/j.cnki.1673-7148.2018.04.001.
[22] Y. W. Wang, X. N. Song, B. H. Tang, Z. L. Li, and P. Leng, "Validation of FY−2C derived land surface temperature over the source region of the Yellow river: A case study of Maqu county," *Remote Sens. Land Resour.*, vol. 27, no. 4, pp. 68–72, Dec. 2015, doi: 10.6046/gtzyyg.2015.04.11.
[23] C. Coll et al., "Long-term accuracy assessment of land surface temperatures derived from the Advanced along-track scanning radiometer," *Remote Sens. Environ.*, vol. 116, pp. 211–225, Jan. 2012, doi: 10.1016/j.rse.2010.01.027.
[24] Z. X. Peng, J. Zhou, and M. S. Li, "Review of methods for simulating land surface temperature at the pixel scale based on ground measurements over heterogeneous surface," *Adv. Earth Sci.*, vol. 31, no. 5, pp. 471–480, 2016, doi: 1011867 /j.issn.1001-8166.2016.05.0471.
[25] F. Arabi Aliabad, M. Zare, and H. G. Malamiri, "Comparison of the accuracy of daytime land surface temperature retrieval methods using Landsat 8 images in arid regions," *Infrared Phys. Technol.*, vol. 115, Jun. 2021, Art. no. 103692, doi: 10.1016/j.infrared.2021.103692.
[26] C. Coll et al., "Laboratory calibration and field measurement of land surface temperature and emissivity using thermal infrared multiband radiometers," *Int. J. Appl. Earth Observation Geoinformation*, vol. 78, pp. 227–239, Jun. 2019, doi: 10.1016/j.jag.2019.02.002.
[27] B. H. Tang, "Nonlinear split-window algorithms for wstimating land and sea surface temperatures from simulated Chinese Gaofen-5 satellite data," *IEEE Trans. Geosci. Remote Sens.*, vol. 56, no. 11, pp. 6280–6289, Nov. 2018, doi: 10.1109/TGRS.2018.2833859.
[28] P. C. Guillevic et al., "Land surface temperature product validation using NOAA's surface climate observation networks—Scaling methodology for the visible infrared imager radiometer suite (VIIRS)," *Remote Sens. Environ.*, vol. 124, pp. 282–298, Sep. 2012, doi: 10.1016/j.rse.2012.05.004.
[29] J. M. Norman and F. Becker, "Terminology in thermal infrared remote sensing of natural surfaces," *Agricultural Forest Meteorol.*, vol. 77, no. 3, pp. 153–166, Dec. 1995, doi: 10.1016/0168-1923(95)02259-Z.
[30] C. Duffour, A. Olioso, J. Demarty, C. Van der Tol, and J. P. Lagouarde, "An evaluation of SCOPE: A tool to simulate the directional anisotropy of satellite-measured surface temperatures," *Remote Sens. Environ.*, vol. 158, pp. 362–375, Mar. 2015, doi: 10.1016/j.rse.2014.10.019.
[31] S. L. Ermida, I. F. Trigo, C. C. DaCamara, F. M. Göttsche, F. S. Olesen, and G. Hulley, "Validation of remotely sensed surface temperature over an oak woodland landscape — The problem of viewing and illumination geometries," *Remote Sens. Environ.*, vol. 148, pp. 16–27, May 2014, doi: 10.1016/j.rse.2014.03.016.

Yiyao Gao received the B.S. degree in surveying and mapping engineering from Suqian University, Jiangsu, China, in 2021. She is currently working toward the M.S. degree in geomatics engineering with the Nanjing University of Information Science and Technology, Nanjing, China.

Her current research interest includes applications of thermal infrared remote sensing.

Shanyou Zhu received the M.S. degree in mineral resource prospecting and exploration from Shandong University of Science and Technology, Taian, China, in 2003, and the Ph.D. degree in electromagnetic field and microwave technology from Shanghai Institute of Technical Physics, Chinese Academy of Sciences, Shanghai, China, in 2006.

He is currently a Professor with the Nanjing University of Information Science and Technology, Nanjing, China. His research interests include the basic theory and application of thermal infrared remote sensing and environmental remote sensing.

Guixin Zhang received the M.S. degree in hydraulics and river dynamics from Hebei University of Engineering, Shijiazhuang, China, in 2006, and the Ph.D. degree in hydrology and water resources from Hohai University, Nanjing, China, in 2017.

She is currently a Lecturer with the Nanjing University of Information Science and Technology, Nanjing, China. Her research interest includes remote sensing applications in meteorology.

Yongming Xu received the M.S. degree in cartography and geographical information system from Institute of Remote Sensing Application, Chinese Academy of Sciences, Beijing, China, in 2005, and the Ph.D. degree in resources and environmental remote sensing from Nanjing University, Nanjing, China, in 2010.

He is currently a Professor with the Nanjing University of Information Science and Technology, Nanjing, China. His research interests include thermal infrared remote sensing, environmental remote sensing, and nighttime lights remote sensing.